CHAPTER 4

Ridge waveguide's optical confinement analysis

We have seen in chapter 3 that presents a three-layer slab-waveguide problem for the conventional DH laser and the index-guided analysis for a lateral structure. This chapter's scheme is to provide both transverse and lateral mode examinations corresponding to the ridge waveguide (RW) structure. The optical confinement analysis of RW plays an attention on the residual thickness (t) of upper cladding layer (see Fig. 2.5) which controls the effective refractive index of the outside-ridge or *wing region* (n_{wing}), while the ridge region, containing very thick upper cladding layer, justifies the residual thickness to be infinity.

In this chapter, we will examine the DH, LOC and SCH transverse structures in the functions of the residual thickness (t) and also analyze the lateral confinement in the functions of ridge width (w) and lateral index step (Δn_L). Further, the *cold-cavity* modes, which is determined while a laser diode is *not operated* (no injected current), are often influenced by external pumping that changes both the gain and the index of refraction. The significant variation in refractive index with external pumping (the injected current density J) is unique to a laser diode and affects its operating characteristics [8,54] in the important way. Finally, a proposed structure used in this thesis is submitted.

4.1 Transverse analysis of DH structure

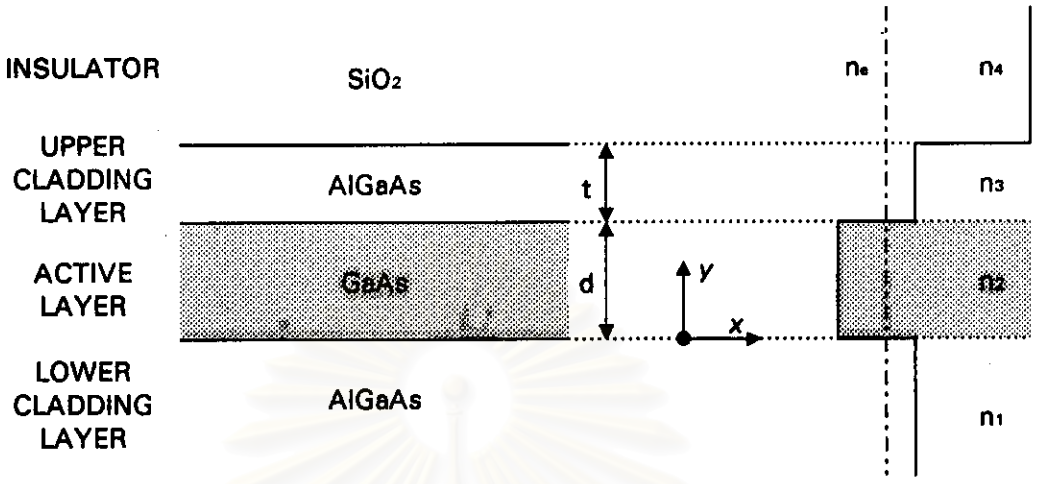

Fig. 4.1 Schematic and index profile of a DH structure corresponding to the wing region of ridge waveguide laser. Shaded area designates the guiding region.

It is different from the DH problem in section 3.4 that concentrates only three layers, i.e. active, lower cladding and upper cladding layers. This structure accounts for the thickness of upper cladding and insulator (SiO_2) layers illustrated in Fig. 4.1. The problem is determined as a four-layer slab-waveguide having a general solution of Eq. (3.11) as following

$$E_y(y) = \begin{cases} A_1 e^{-\gamma_1 y} + A_2 e^{\gamma_1 y} & , y \le 0 \\ B_1 \cos(\kappa y) + B_2 \sin(\kappa y) & , 0 \le y \le d \\ C_1 e^{-\gamma_3 y} + C_2 e^{\gamma_3 y} & , d \le y \le (d+t) \\ D_1 e^{-\gamma_4 y} + D_2 e^{\gamma_4 y} & , (d+t) \le y \end{cases} \qquad (4.1)$$

where

$$\gamma_1 = k_o (n_e^2 - n_1^2)^{1/2} \qquad (4.2)$$

$$\kappa = k_o (n_2^2 - n_e^2)^{1/2} \qquad (4.3)$$

$$\gamma_3 = k_o (n_e^2 - n_3^2)^{1/2} \qquad (4.4)$$

$$\gamma_4 = k_o (n_e^2 - n_4^2)^{1/2} \qquad (4.5)$$

and n_1, n_2, n_3 and n_4 are the material refractive indices for the lower cladding, active, upper cladding and insulator, respectively, with the index profile $n_2 > n_1$, n_3 and n_4 shown in Fig. 4.1.

By applying boundary conditions with the same procedure of section 3.4, we obtain the eigenvalue equation

$$\begin{bmatrix} 1 & -1 & 0 & 0 & 0 & 0 \\ \gamma_1 & 0 & -\kappa & 0 & 0 & 0 \\ 0 & \cos(\kappa d) & \sin(\kappa d) & -e^{-\gamma_3 d} & -e^{\gamma_3 d} & 0 \\ 0 & -\kappa\sin(\kappa d) & \kappa\cos(\kappa d) & \gamma_3 e^{-\gamma_3 d} & -\gamma_3 e^{\gamma_3 d} & 0 \\ 0 & 0 & 0 & e^{-\gamma_3(d+t)} & e^{\gamma_3(d+t)} & -e^{-\gamma_4(d+t)} \\ 0 & 0 & 0 & -\gamma_3 e^{-\gamma_3(d+t)} & \gamma_3 e^{\gamma_3(d+t)} & \gamma_4 e^{-\gamma_4(d+t)} \end{bmatrix} \begin{bmatrix} A_2 \\ B_1 \\ B_2 \\ C_1 \\ C_2 \\ D_1 \end{bmatrix} = 0 \qquad (4.6)$$

whose solutions achieved by numerical calculation taking the determinant of 6×6 matrix to be zero. The resultant effective indices must satisfy the inequality $n_2 > n_e > n_1$, n_3 and n_4.

The confinement factor (Γ_T) is carried out by

$$\Gamma_T = \frac{\int_0^d E_y^2(y)\,dy}{\int_{-\infty}^{\infty} E_y^2(y)\,dy} \qquad (4.7)$$

Using of the structure in Fig. 4.1 with constant active-layer index and varied cladding-layer indices, effective refractive index (n_e) and transverse confinement factor (Γ_T) are obtained as shown in Fig. 4.2. In each figure, the profiles of both values increase and tend to be constant within the concerned residual thickness of 1.2 μm. From the figure comparison, the index difference of active and cladding layer (n_2-n_1), which is originated by increasing cladding-layer index, produces less confined power ranged from 33% to 18% shown in Fig. 4.2a to 4.2d and also produces higher effective refractive indices.

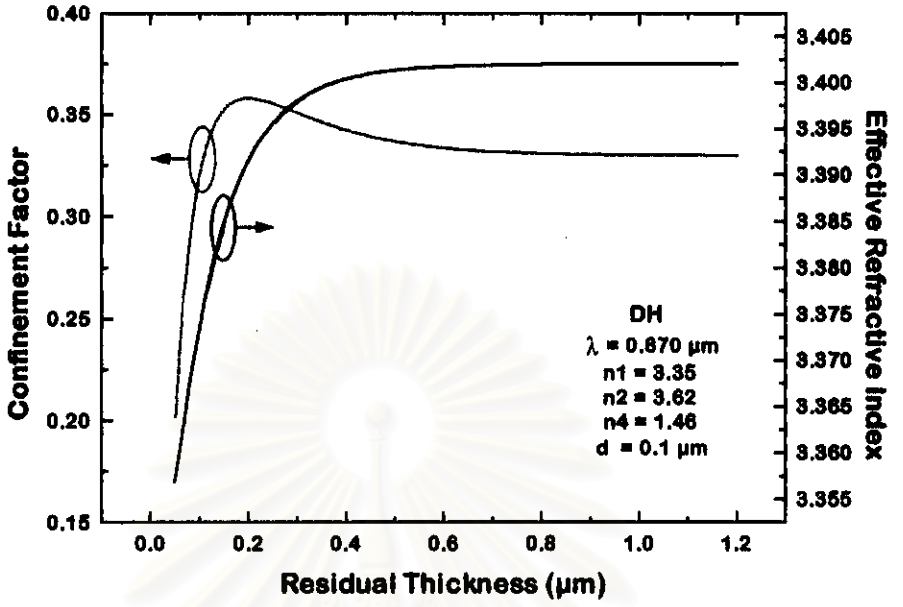

(a)

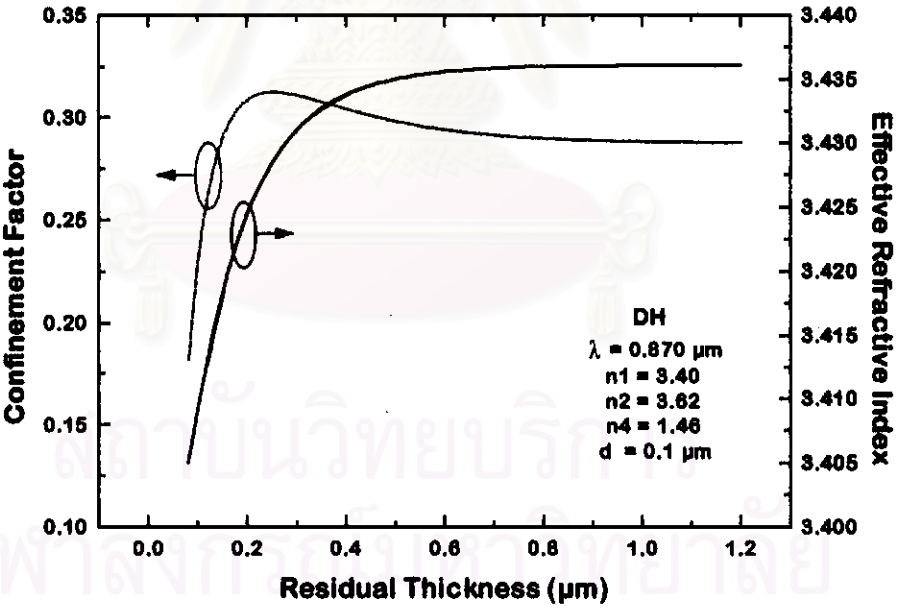

(b)

Fig. 4.2 Simulation results of transverse confinement factor (Γ_T) and effective refractive index (n_e) as the functions of the residual upper cladding layer thickness (t) for 0.870 μm GaAs DH lasers with varied cladding-layer indices (a) 3.35, (b) 3.40, (c) 3.45 and (d) 3.50. The solid and dotted line are represented to effective refractive index and confinement factor, respectively.

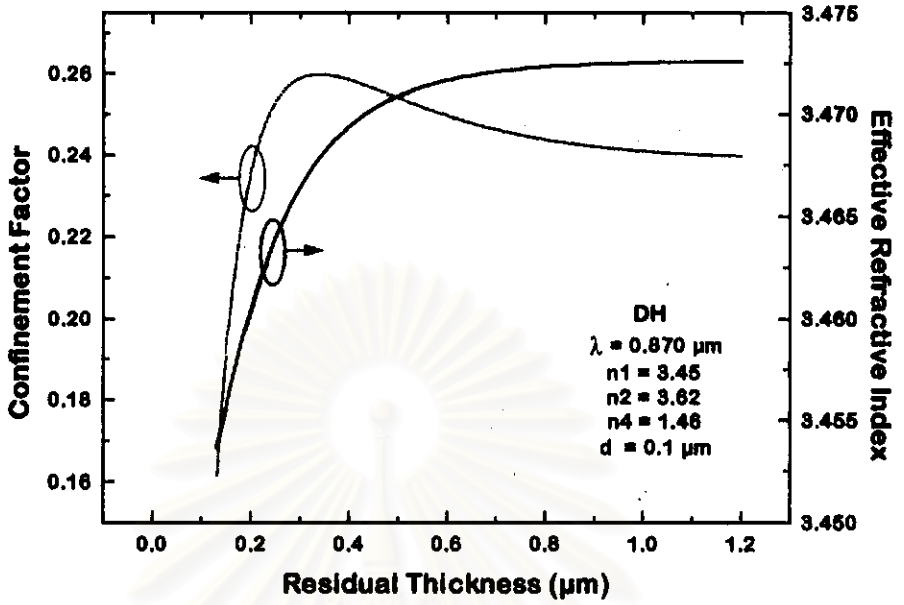

(c)

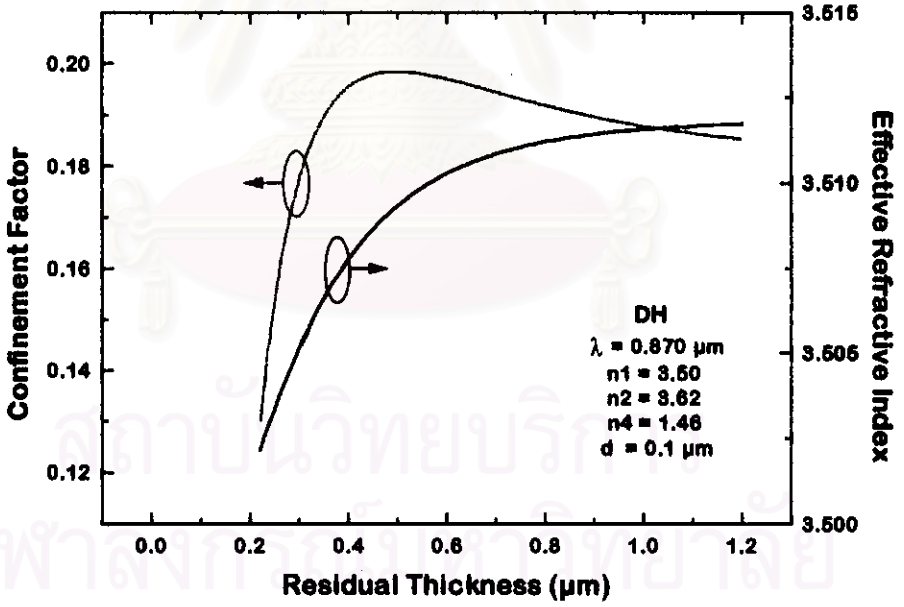

(d)

Fig. 4.2 (cont.) Simulation results of transverse confinement factor (Γ_T) and effective refractive index (n_e) as the functions of the residual upper cladding layer thickness (t) for 0.870 μm GaAs DH lasers with varied cladding-layer indices (a) 3.35, (b) 3.40, (c) 3.45 and (d) 3.50. The solid and dotted line are represented to effective refractive index and confinement factor, respectively.

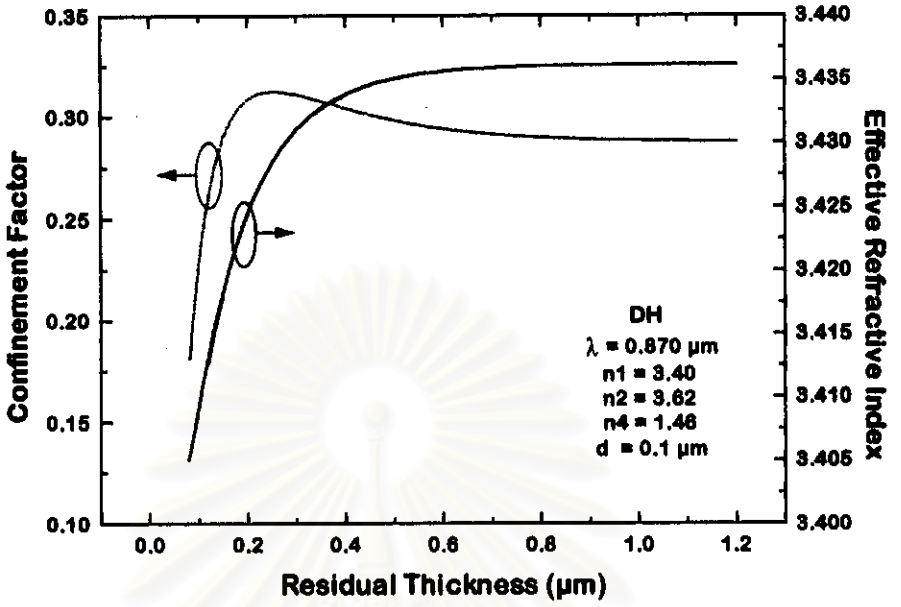

(a)

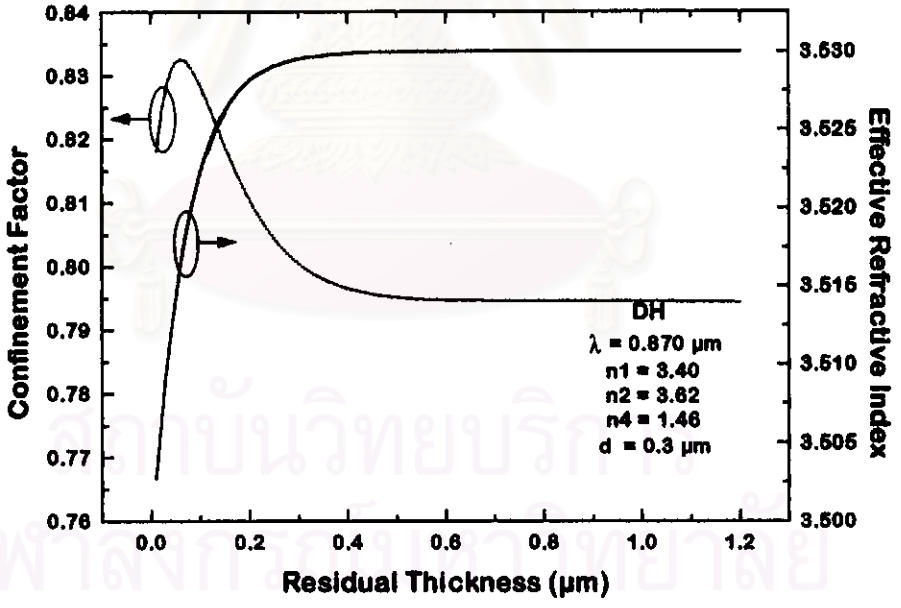

(b)

Fig. 4.3 Simulation results of transverse confinement factor (Γ_T) and effective refractive index (n_e) as the functions of the residual upper cladding layer thickness (t) for 0.870 μm GaAs DH lasers with varied active layer thickness (a) 0.1, (b) 0.3 and (c) 0.5 μm. In the latter case, two optical modes are occurred due to the large active layer thickness. The solid and dotted line are represented to effective refractive index and confinement factor, respectively.

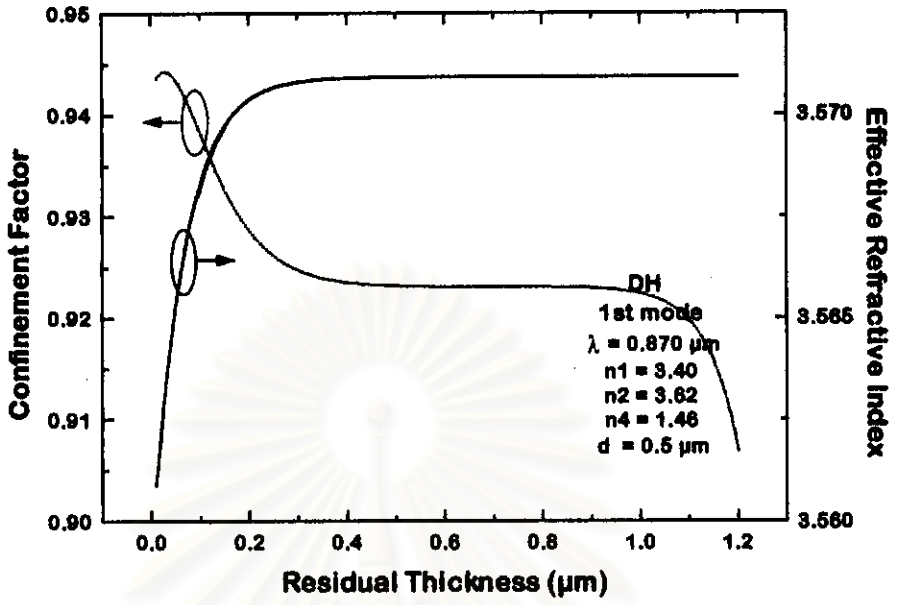

(c-1)

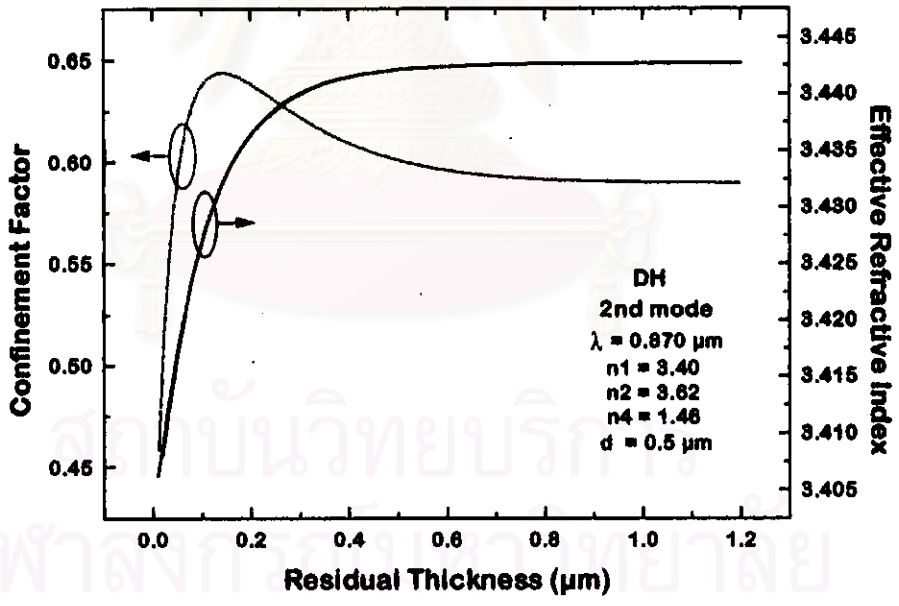

(c-2)

Fig. 4.3 (cont.) Simulation results of transverse confinement factor (Γ_T) and effective refractive index (n_e) as the functions of the residual upper cladding layer thickness (t) for 0.870 μm GaAs DH lasers with varied active layer thickness (a) 0.1, (b) 0.3 and (c) 0.5 μm. In the latter case, two optical modes are occurred due to the large active layer thickness. The solid and dotted line are represented to effective refractive index and confinement factor, respectively.

Fig 4.3 shows the simulation results of the DH laser as the functions of the residual thickness (t) with varied active-layer thickness (d) while both active- and cladding-layers indices (n_2 and n_1) are constantly set to 3.62 and 3.40 respectively. It is reasonable that the larger active-layer thickness presents higher confinement factor ranged from 30% to 92% shown in Fig. 4.3a to 4.3c. Although more than 90% confinement factor is achieved by 0.5 μm active-layer thickness (Fig. 4.3c), but an undesired higher mode is occurred as shown in Fig. 4.3c-2 which reduces the portion of fundamental-mode output power.

4.2 Transverse analysis of LOC structure

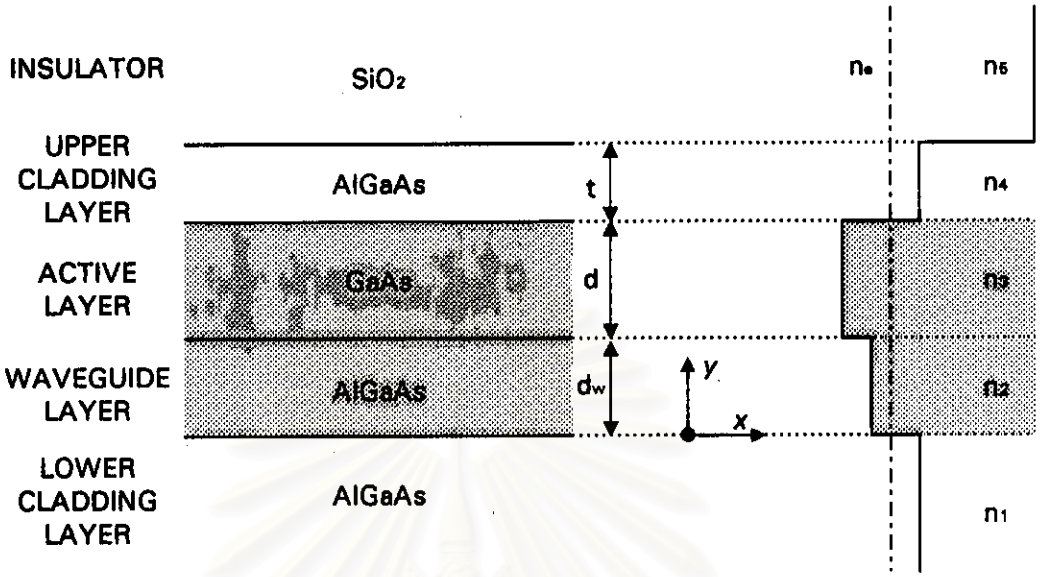

Fig. 4.4 Schematic and index profile of a type-A LOC structure corresponding to the wing region of ridge waveguide laser. Shaded area designates the guiding region.

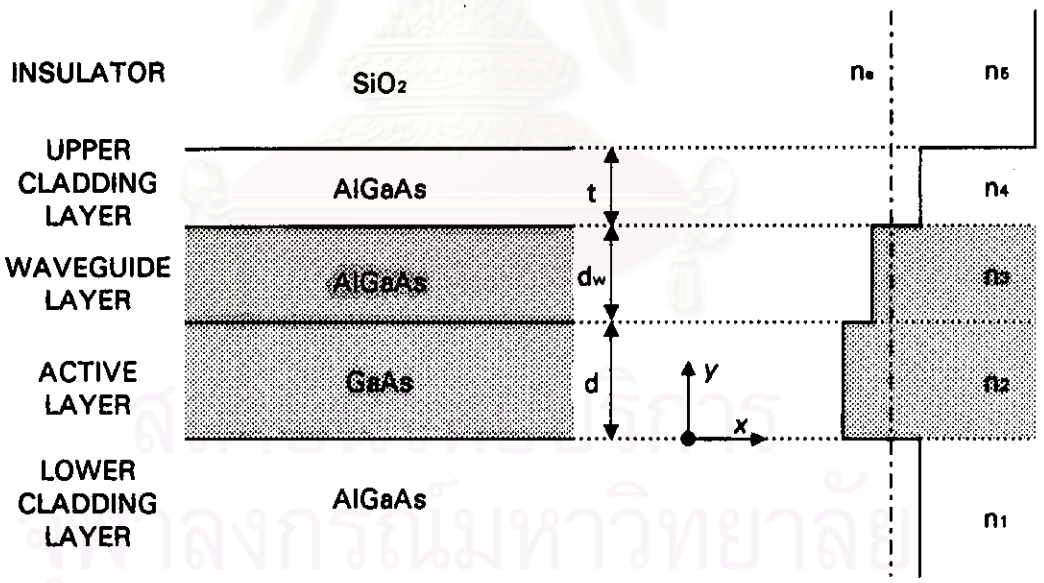

Fig. 4.5 Schematic and index profile of a type-B LOC structure corresponding to the wing region of ridge waveguide laser. Shaded area designates the guiding region.

The additions of a waveguiding layer in the LOC structure have twofold, type-A and type-B which place the waveguiding layer under and above the active layer

schematically shown in Fig. 4.4 and 4.5 respectively. Both structures produce the two sets of the five-layer problems. The type-A solution is of the form

$$E_y(y) = \begin{cases} A_1 e^{-\gamma_1 y} + A_2 e^{\gamma_1 y} & , y \le 0 \\ B_1 \cos(\kappa_w y) + B_2 \sin(\kappa_w y) & , 0 \le y \le d_w \\ C_1 \cos(\kappa y) + C_2 \sin(\kappa y) & , d \le y \le (d_w + d) \\ D_1 e^{-\gamma_4 y} + D_2 e^{\gamma_4 y} & , (d_w + d) \le y \le (d_w + d + t) \\ E_1 e^{-\gamma_5 y} + E_2 e^{\gamma_5 y} & , (d_w + d + t) \le y \end{cases} \quad (4.8)$$

where

$$\gamma_1 = k_o (n_e^2 - n_1^2)^{1/2} \quad (4.9)$$

$$\kappa_w = k_o (n_2^2 - n_e^2)^{1/2} \quad (4.10)$$

$$\kappa = k_o (n_3^2 - n_e^2)^{1/2} \quad (4.11)$$

$$\gamma_4 = k_o (n_e^2 - n_4^2)^{1/2} \quad (4.12)$$

$$\gamma_5 = k_o (n_e^2 - n_5^2)^{1/2} \quad (4.13)$$

and n_1, n_2, n_3, n_4 and n_5 are the material refractive indices for the lower cladding, waveguiding, active, upper cladding and insulator, respectively. The eigenvalue equation is carried out by eight boundary equations. The confined mode in type-A LOC laser must look upon both active and waveguiding layers, thus the dividend of the confinement factor equation [Eq.(3.14)] is integrated over 0 to $d_w + d$.

$$\Gamma_T = \frac{\int_0^{d_w + d} E_y^2(y)\, dy}{\int_{-\infty}^{\infty} E_y^2(y)\, dy} \quad (4.14)$$

The solutions of this type-A structure is shown in Fig. 4.6. By constantly setting the indices of active-layer (n_3) and insulator (n_5) to 3.62 and 1.46, and setting the thickness of active- (d) and waveguiding-layer (d_w) to 0.1 μm and 0.4 μm, there are two majors found from the result comparison. First, at the same cladding-layer indices (n_1), more confined power is obtained by increasing the waveguiding-layer index (n_2). Second, at the same waveguiding-layer index (n_2), more confined power is obtained by decreasing the cladding-layer indices (n_1). It means that the higher index difference between the cladding layer and guiding region, consisted of the active and waveguiding layers, causes the higher level of optical confinement factor.

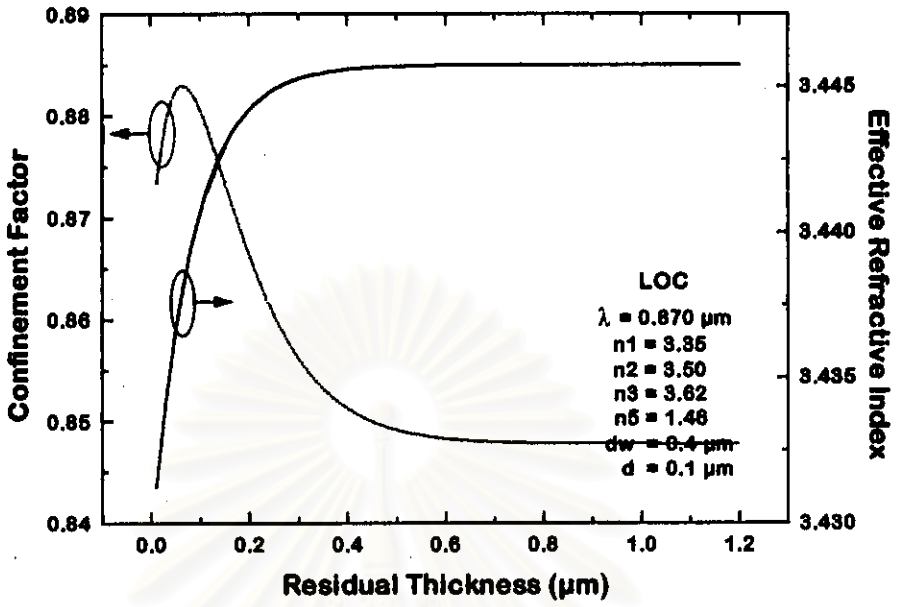

(a)

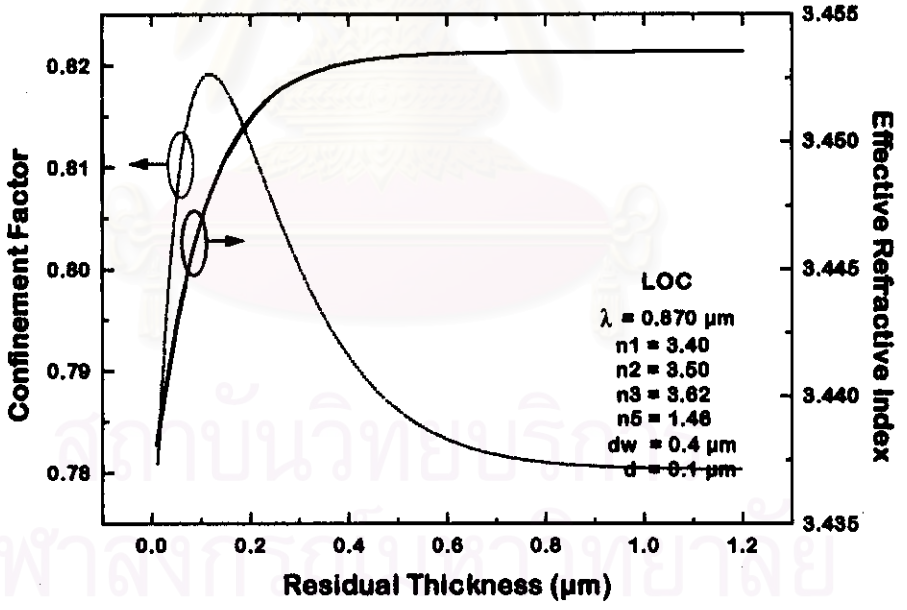

(b)

Fig. 4.6 Simulation results of transverse confinement factor (Γ_T) and effective refractive index (n_e) as the functions of the residual upper cladding layer thickness (t) for 0.870 μm GaAs type-A LOC lasers with varied cladding- and waveguiding-layers indices, n_1 and n_2, (a) n_1=3.35 and n_2=3.50, (b) n_1=3.40 and n_2=3.50, (c) n_1=3.35 and n_2=3.45 and (d) n_1=3.40 and n_2=3.45. The solid and dotted line are represented to effective refractive index and confinement factor, respectively.

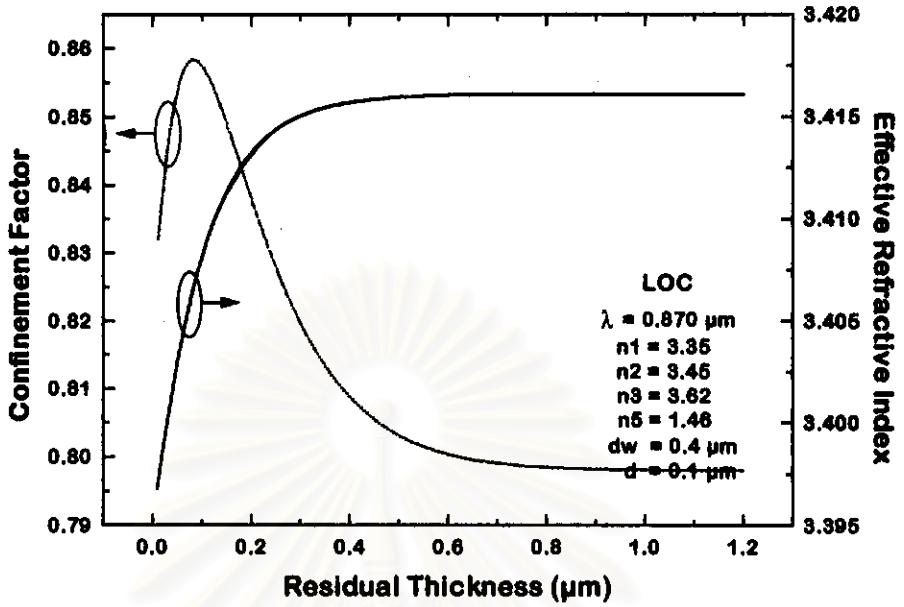

(c)

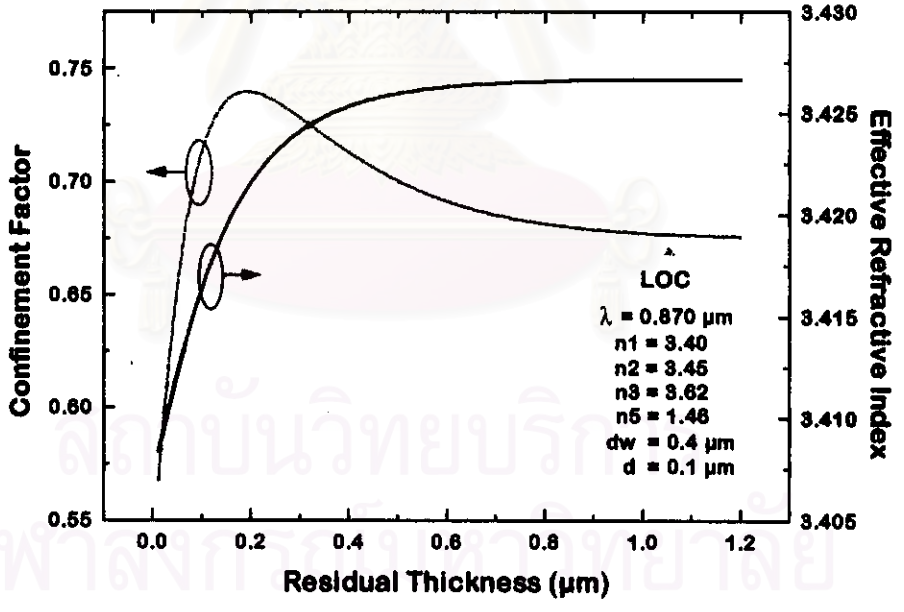

(d)

Fig. 4.6 (cont.) Simulation results of transverse confinement factor (Γ_T) and effective refractive index (n_e) as the functions of the residual upper cladding layer thickness (t) for 0.870 μm GaAs type-A LOC lasers with varied cladding- and waveguiding-layers indices, n_1 and n_2, (a) n_1=3.35 and n_2=3.50, (b) n_1=3.40 and n_2=3.50, (c) n_1=3.35 and n_2=3.45 and (d) n_1=3.40 and n_2=3.45. The solid and dotted line are represented to effective refractive index and confinement factor, respectively.

For the type-B structure, the solution is of the form

$$E_y(y) = \begin{cases} A_1 e^{-\gamma_1 y} + A_2 e^{\gamma_1 y} & , y \le 0 \\ B_1 \cos(\kappa y) + B_2 \sin(\kappa y) & , 0 \le y \le d \\ C_1 \cos(\kappa_w y) + C_2 \sin(\kappa_w y) & , d \le y \le (d + d_w) \\ D_1 e^{-\gamma_4 y} + D_2 e^{\gamma_4 y} & , (d + d_w) \le y \le (d+d_w+t) \\ E_1 e^{-\gamma_5 y} + E_2 e^{\gamma_5 y} & , (d+d_w+t) \le y \end{cases} \quad (4.15)$$

where

$$\gamma_1 = k_o (n_e^2 - n_1^2)^{1/2} \quad (4.16)$$

$$\kappa = k_o (n_2^2 - n_e^2)^{1/2} \quad (4.17)$$

$$\kappa_w = k_o (n_3^2 - n_e^2)^{1/2} \quad (4.18)$$

$$\gamma_4 = k_o (n_e^2 - n_4^2)^{1/2} \quad (4.19)$$

$$\gamma_5 = k_o (n_e^2 - n_5^2)^{1/2} \quad (4.20)$$

And the confinement factor equation is carried out by integrating over 0 to $d + d_w$.

$$\Gamma_T = \frac{{}_0\int^{d+d_w} E_y^2(y)\, dy}{{}_{-\infty}\int^{\infty} E_y^2(y)\, dy} \quad (4.21)$$

Fig. 4.7 shows the simulation results of this type-B structure which use the same parameters (both indices and thickness) as type-A, except the location of the waveguiding layer. The figures reveal the same conclusion as type-A that the higher index difference between cladding layer and guiding region causes the higher confined power.

By comparing type-A to type-B, at the waveguiding index (n_3) of 3.50, the type-A LOC lasers have slightly higher confinement factor than type-B's, while at the waveguiding index of 3.45, the type-B ones have higher results than type-A's. This situation can imply that the electromagnetic wave distribution, causing the confinement factor, in LOC structure is much strongly depending on the index profile than depending on the location of waveguiding layer.

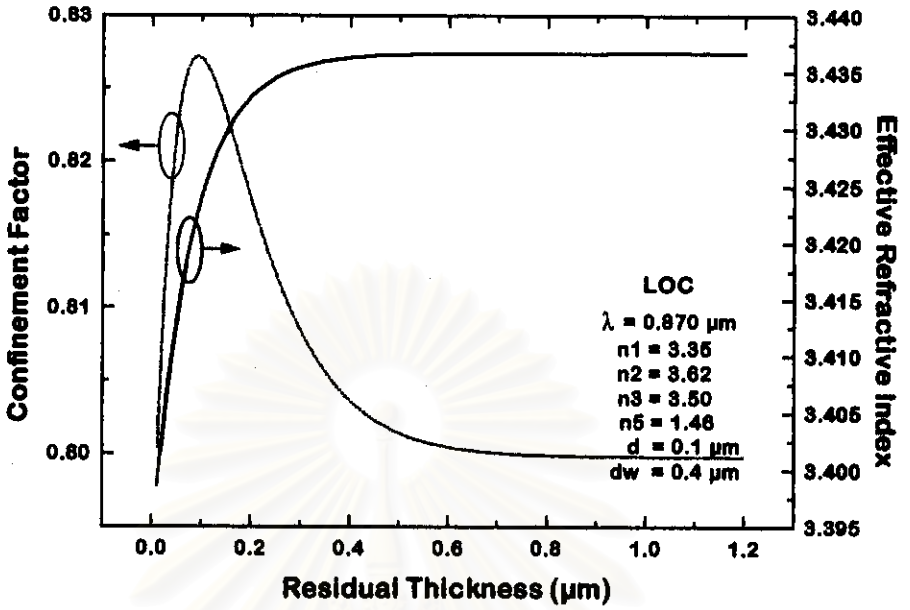

(a)

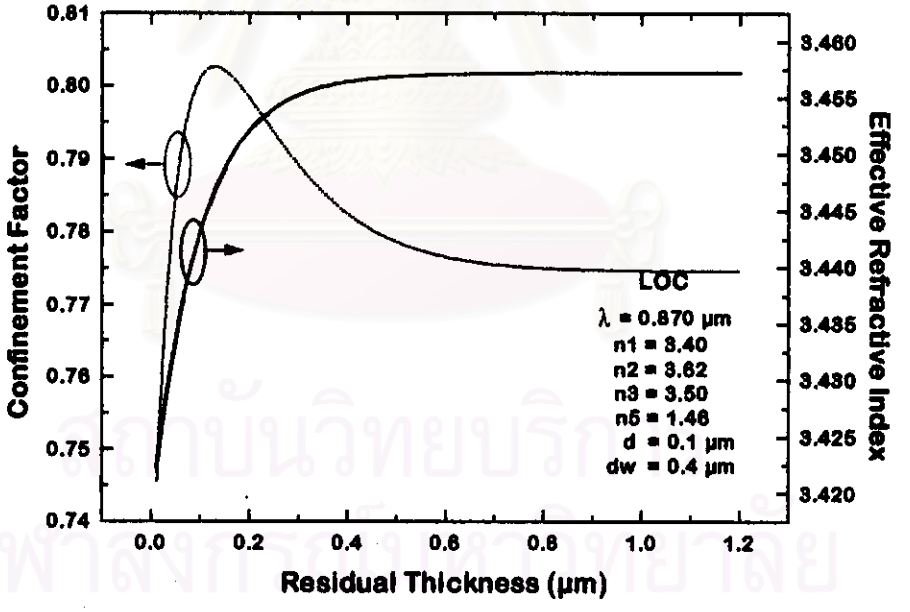

(b)

Fig. 4.7 Simulation results of transverse confinement factor (Γ_T) and effective refractive index (n_e) as the functions of the residual upper cladding layer thickness (t) for 0.870 μm GaAs type-B LOC lasers with varied cladding- and waveguiding-layers indices, n_1 and n_3, (a) n_1=3.35 and n_3=3.50, (b) n_1=3.40 and n_3=3.50, (c) n_1=3.35 and n_3=3.45 and (d) n_1=3.40 and n_3=3.45. The solid and dotted line are represented to effective refractive index and confinement factor, respectively.

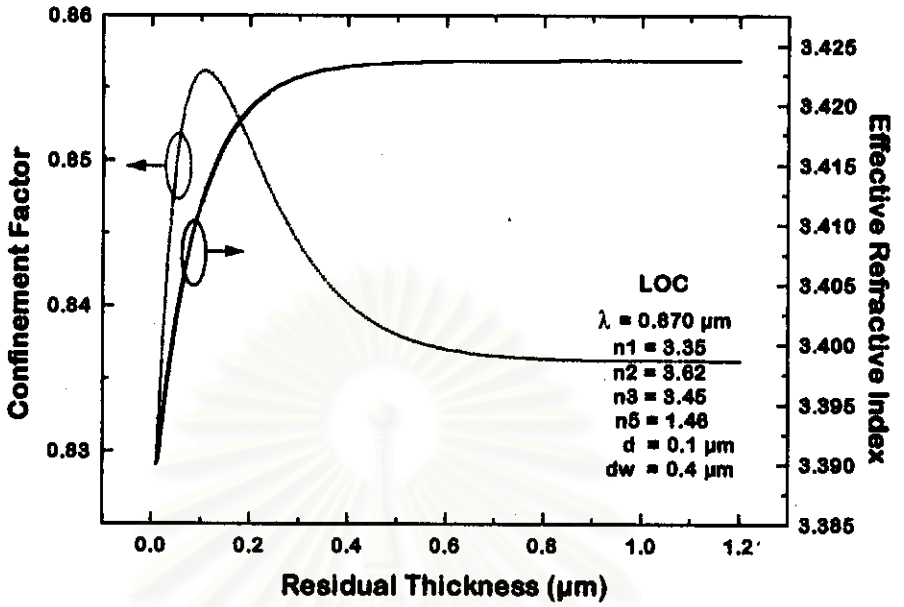

(c)

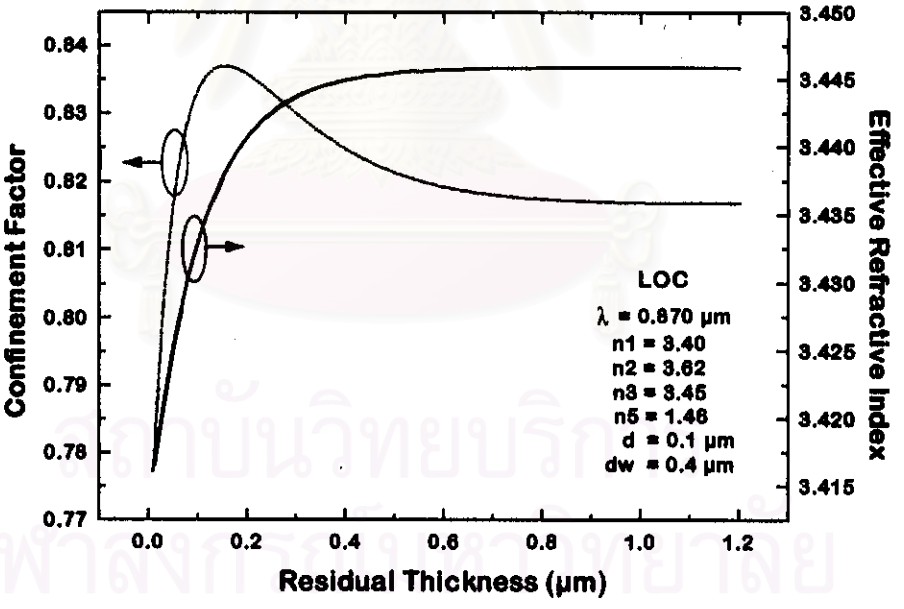

(d)

Fig. 4.7 (cont.) Simulation results of transverse confinement factor (Γ_T) and effective refractive index (n_e) as the functions of the residual upper cladding layer thickness (t) for 0.870 μm GaAs type-B LOC lasers with varied cladding- and waveguiding-layers indices, n_1 and n_3, (a) n_1=3.35 and n_3=3.50, (b) n_1=3.40 and n_3=3.50, (c) n_1=3.35 and n_3=3.45 and (d) n_1=3.40 and n_3=3.45. The solid and dotted line are represented to effective refractive index and confinement factor, respectively.

4.3 Transverse analysis of SCH structure

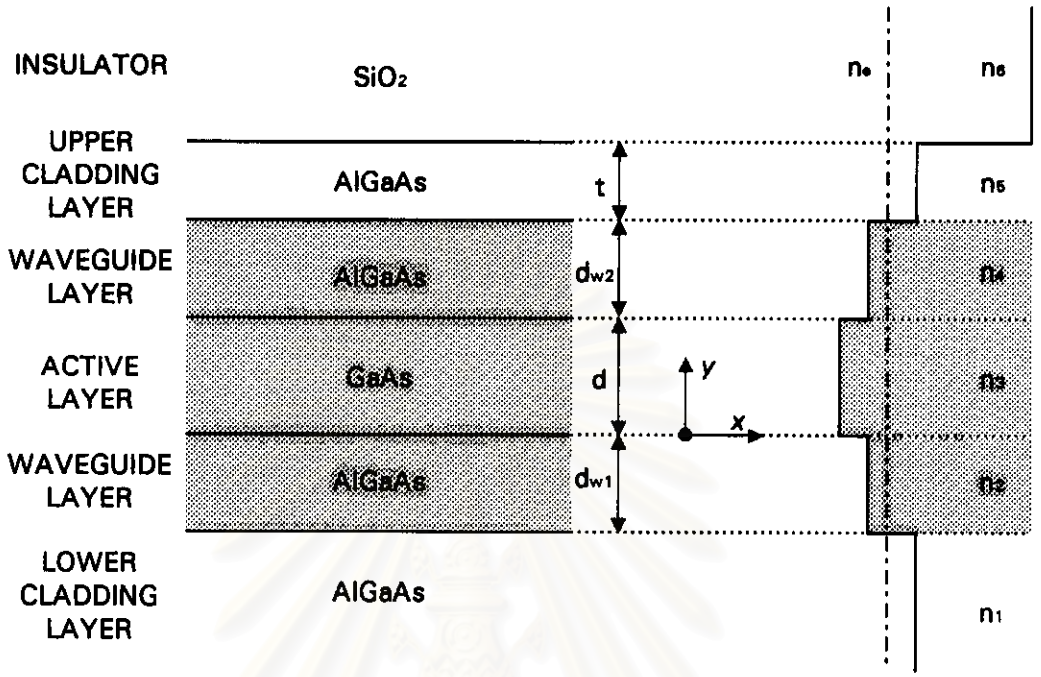

Fig. 4.8 Schematic and index profile of a SCH structure corresponding to the wing region of ridge waveguide laser. Shaded area designates the guiding region.

The SCH laser diode contains two waveguiding layers sandwiching the active layer and sandwiched by two cladding layers. The solution of the transverse field equation [Eq.(3.11)], carried out from six-layer structure schematically illustrated in Fig. 4.8, is shown in consequent equations

$$E_y(y) = \begin{cases} A_1 e^{-\gamma_1 y} + A_2 e^{\gamma_1 y} & , \; y \le -d_{w1} \\ B_1 \cos(\kappa_{w1} y) + B_2 \sin(\kappa_{w1} y) & , \; -d_{w1} \le y \le 0 \\ C_1 \cos(\kappa y) + C_2 \sin(\kappa y) & , \; 0 \le y \le d \\ D_1 \cos(\kappa_{w2} y) + D_2 \sin(\kappa_{w2} y) & , \; d \le y \le (d + d_{w2}) \\ E_1 e^{-\gamma_5 y} + E_2 e^{\gamma_5 y} & , \; (d + d_{w2}) \le y \le (d + d_{w2} + t) \\ F_1 e^{-\gamma_6 y} + F_2 e^{\gamma_6 y} & , \; (d + d_{w2} + t) \le y \end{cases} \quad (4.22)$$

where

$$\gamma_1 = k_o (n_e^2 - n_1^2)^{1/2} \quad (4.23)$$

$$\kappa_{w1} = k_o (n_2^2 - n_e^2)^{1/2} \quad (4.24)$$

$$\kappa = k_o (n_3^2 - n_e^2)^{1/2} \quad (4.25)$$

$$\kappa_{w2} = k_o (n_4^2 - n_e^2)^{1/2} \quad (4.26)$$

$$\gamma_5 = k_o (n_e^2 - n_5^2)^{1/2} \quad (4.27)$$

$$\gamma_6 = k_o (n_e^2 - n_6^2)^{1/2} \quad (4.28)$$

and n_1, n_2, n_3, n_4, n_5 and n_6 are the material refractive indices for the lower cladding, lower waveguiding, active, upper waveguiding, upper cladding and insulator, respectively. In the same rhythm of section 4.2, the confinement factor is obtained by

$$\Gamma_T = \frac{\int_{-d_{w1}}^{d_{w2}} E_y^2(y)\, dy}{\int_{-\infty}^{\infty} E_y^2(y)\, dy} \quad (4.29)$$

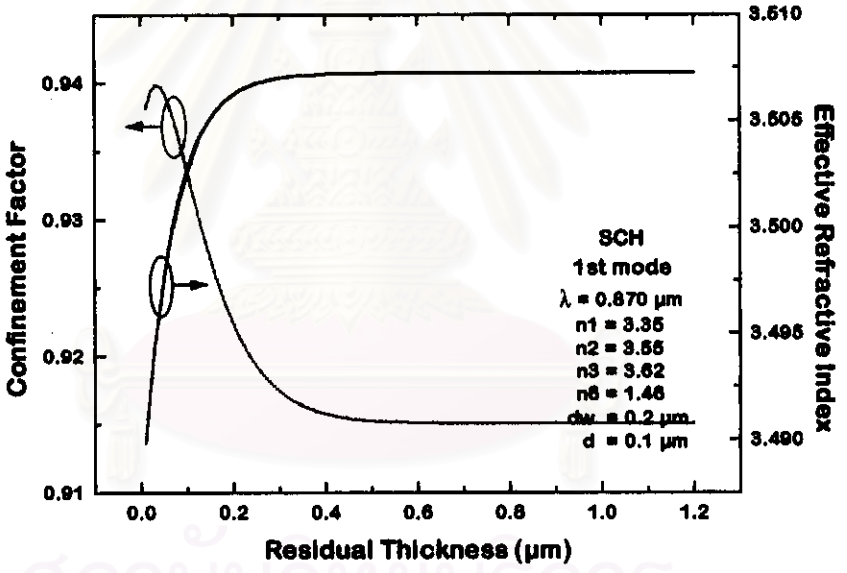

(a-1)

Fig. 4.9 Simulation results of transverse confinement factor (Γ_T) and effective refractive index (n_e) as the functions of the residual upper cladding layer thickness (t) for 0.870 μm GaAs symmetrical SCH lasers with varied cladding- and waveguiding-layer indices, n_1 and n_2, (a) n_1=3.35 and n_2=3.55, (b) n_1=3.35 and n_2=3.55, (c) n_1=3.40 and n_2=3.55 and (d) n_1=3.40 and n_2=3.50. In the first case, two optical modes are occurred due to the large index differences between cladding-layer and waveguiding-region. The solid and dotted line are represented to effective refractive index and confinement factor, respectively.

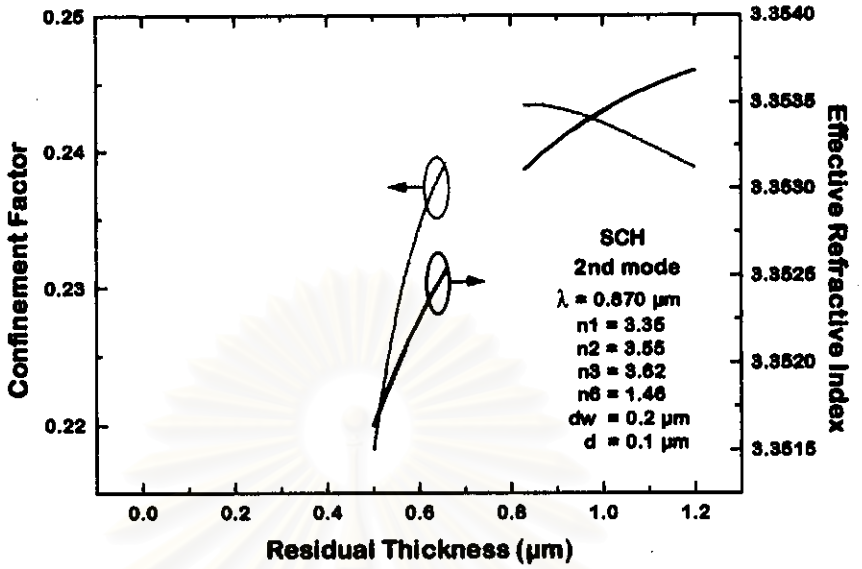

(a-2)

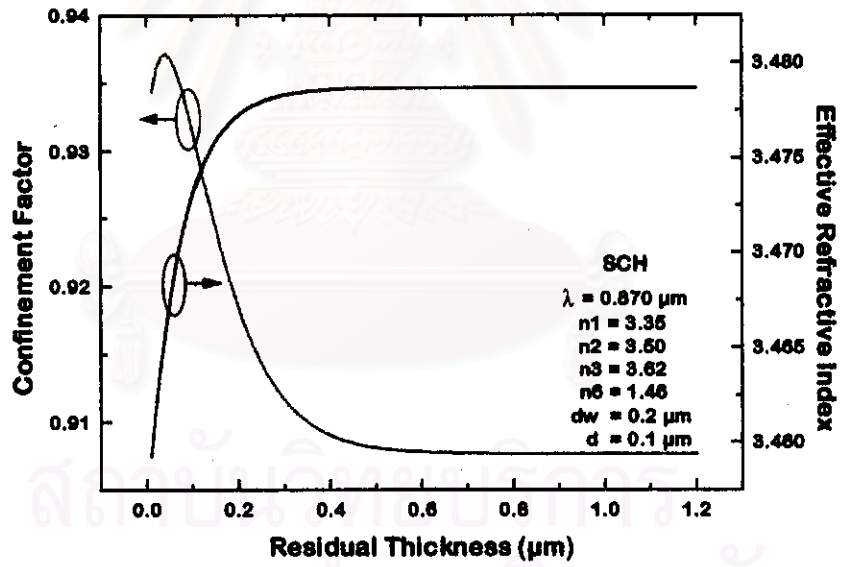

(b)

Fig. 4.9 (cont.) Simulation results of transverse confinement factor (Γ_T) and effective refractive index (n_e) as the functions of the residual upper cladding layer thickness (t) for 0.870 μm GaAs symmetrical SCH lasers with varied cladding- and waveguiding-layer indices, n_1 and n_2, (a) n_1=3.35 and n_2=3.55, (b) n_1=3.35 and n_2=3.55, (c) n_1=3.40 and n_2=3.55 and (d) n_1=3.40 and n_2=3.50. In the first case, two optical modes are occurred due to the large index differences between cladding-layer and waveguiding-region. The solid and dotted line are represented to effective refractive index and confinement factor, respectively.

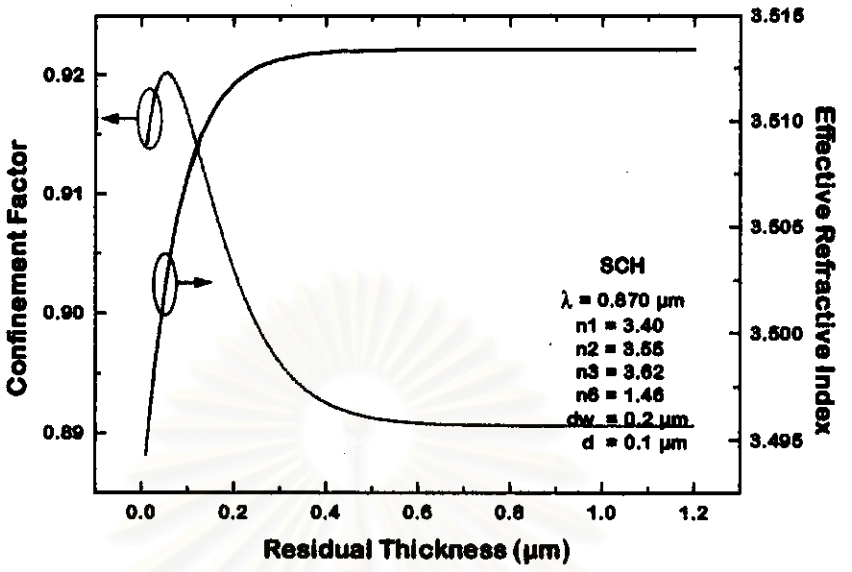

(c)

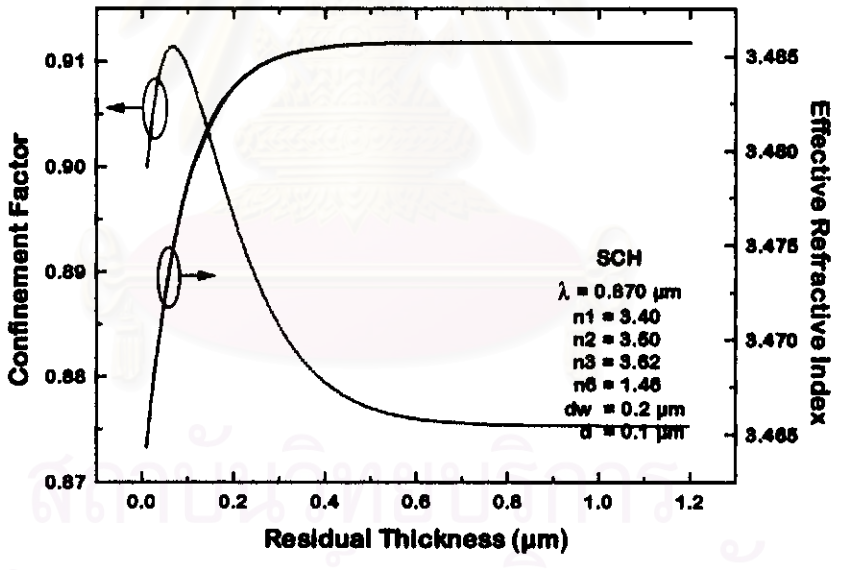

(d)

Fig. 4.9 (cont.) Simulation results of transverse confinement factor (Γ_T) and effective refractive index (n_e) as the functions of the residual upper cladding layer thickness (t) for 0.870 μm GaAs symmetrical SCH lasers with varied cladding- and waveguiding-layer indices, n_1 and n_2, (a) n_1=3.35 and n_2=3.55, (b) n_1=3.35 and n_2=3.55, (c) n_1=3.40 and n_2=3.55 and (d) n_1=3.40 and n_2=3.50. In the first case, two optical modes are occurred due to the large index differences between cladding-layer and waveguiding-region. The solid and dotted line are represented to effective refractive index and confinement factor, respectively.

The solutions of transverse confinement factor (Γ_T) and effective refractive index (n_e) as the functions of residual thickness (t) for the GaAs symmetrical SCH laser, which both material indices and layer thickness of the upper and lower waveguiding layers are equivalent, is shown in Fig. 4.9. In this structure, the guiding region is accounted for an active layer and two waveguiding layers. From the figures, the increased confinement factor can be obtained by the higher index difference between guiding region and cladding layers. But the very high index difference of these two regions can produce an undesired mode shown in Fig. 4.9a-2. The optimum index profile must be considered for a high confined power while maintaining the single mode operation.

Fig. 4.10 shows the comparison among four transverse structures of GaAs lasers, DH, LOC-A, LOC-B and SCH. In the first four simulation results, Fig. 4.10a-4.10d, the active-layer thickness are set to 0.1 μm and using the same material indices for active, cladding and waveguiding layers. The DH structure without waveguiding layer has the least confinement factor of 28%, while the LOC-A, LOC-B and SCH have 76%, 77.5% and 87.5%. The very much optical loss in the DH laser obviously comes from its narrow guiding region of 0.1 μm but in the LOC and SCH the guiding region have 0.5 μm thickness consisted of the active and waveguiding layers. Then 0.5 μm active layer thickness for the DH was calculated and plotted in Fig. 4.10e, the confinement factor increases dramatically (92%) in this case but the second mode also exists which is unpleasant to the single-mode lasers and also reduces the portion of fundamental mode power. Comparing LOC-A to LOC-B structures, type-A is more corresponding to electromagnetic wave profile than type-B because the major crest of the wave is more suitable placed, then the LOC-A have slightly more confined power than the LOC-B. But both of them are still less than SCH about 10% because its active layer which is located in the center of the guiding region (sandwiched by two waveguiding layers) is the most suitable for the wave distribution in laser structure, thus the SCH is the most pleasure structure for optical confinement in this time.

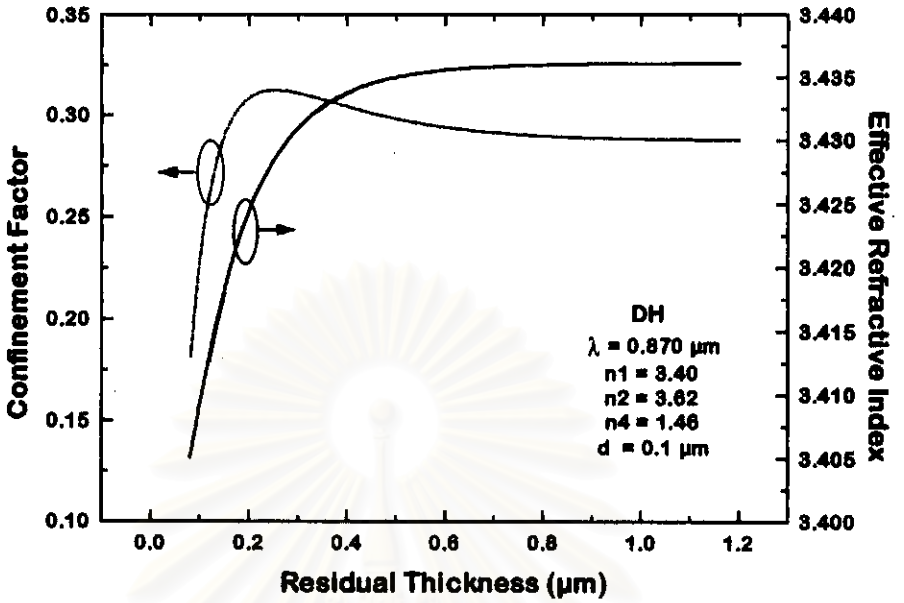

(a)

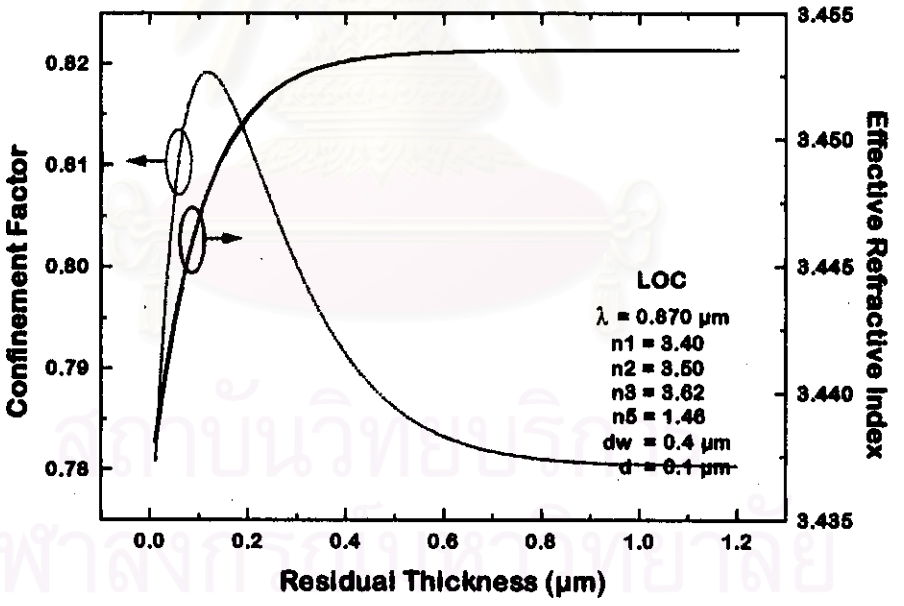

(b)

Fig. 4.10 Comparison of transverse confinement factor (Γ_T) and effective refractive index (n_e) in various transverse structures (a) DH with 0.1 μm active layer thickness, (b) type-A LOC, (c) type-B LOC, (d) SCH and (e) DH with 0.5 μm active layer thickness. The latter case exists two optical modes (e-1) fundamental and (e-2) second modes. The solid and dotted line are represented to effective refractive index and confinement factor, respectively.

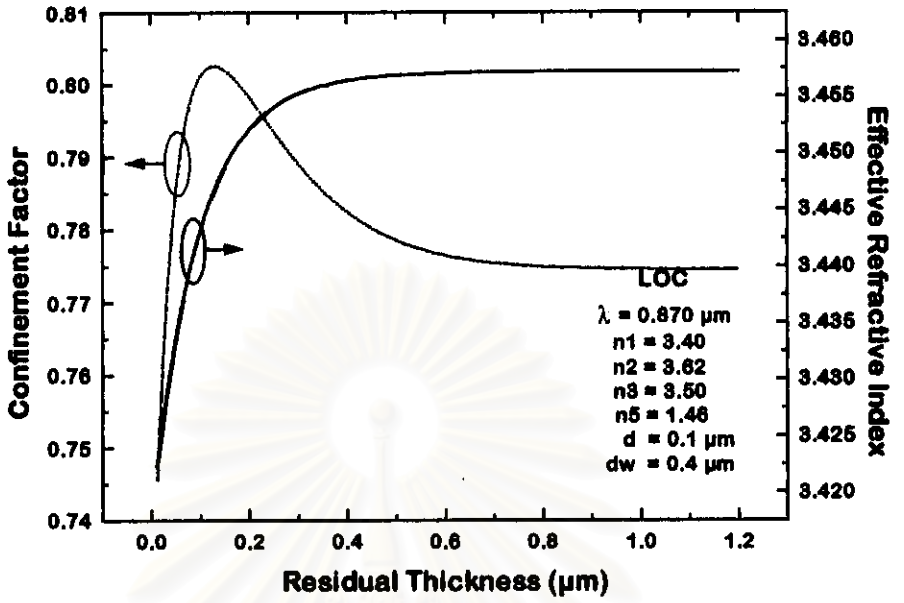

(c)

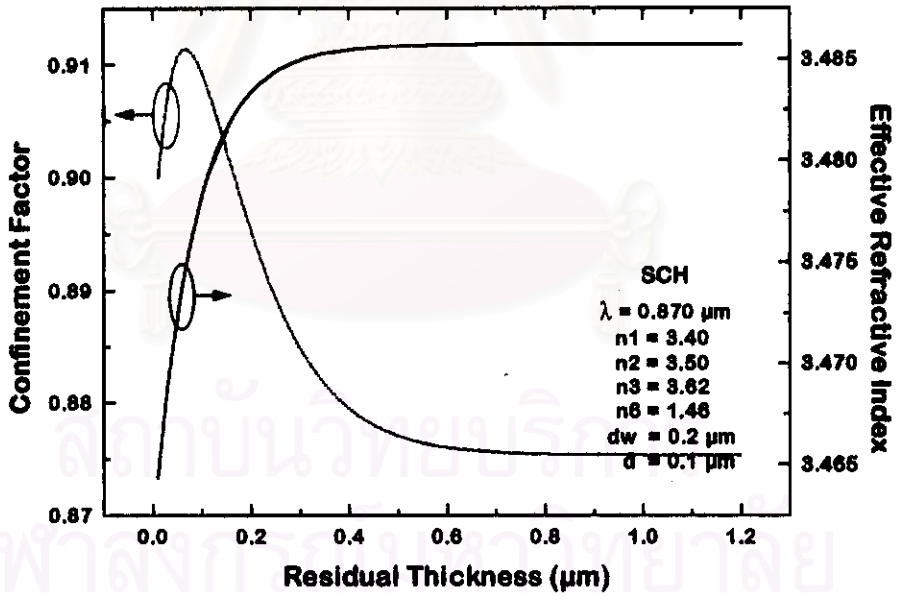

(d)

Fig. 4.10 (cont.) Comparison of transverse confinement factor (Γ_T) and effective refractive index (n_e) in various transverse structures (a) DH with 0.1 μm active layer thickness, (b) type-A LOC, (c) type-B LOC, (d) SCH and (e) DH with 0.5 μm active layer thickness. The latter case exists two optical modes (e-1) fundamental and (e-2) second modes. The solid and dotted line are represented to effective refractive index and confinement factor, respectively.

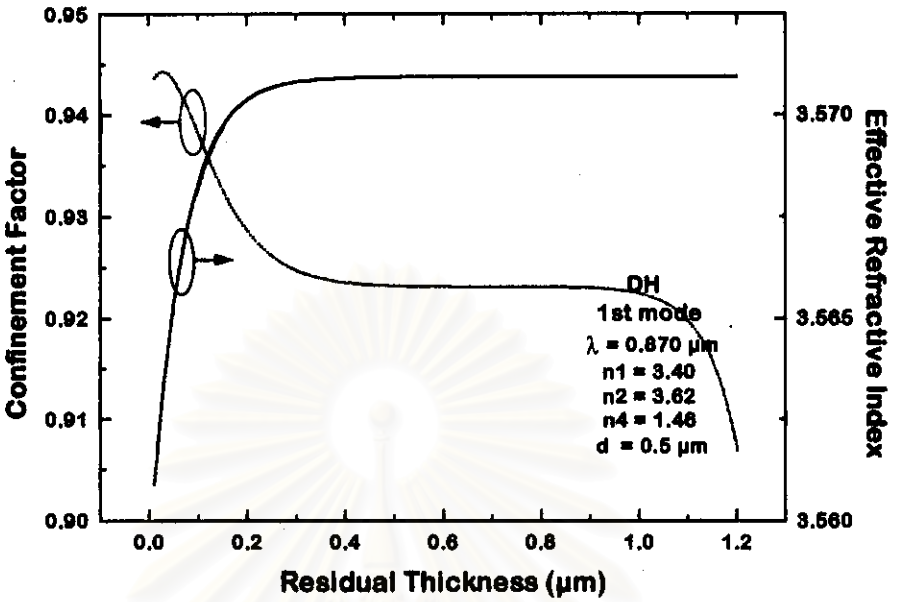

(e-1)

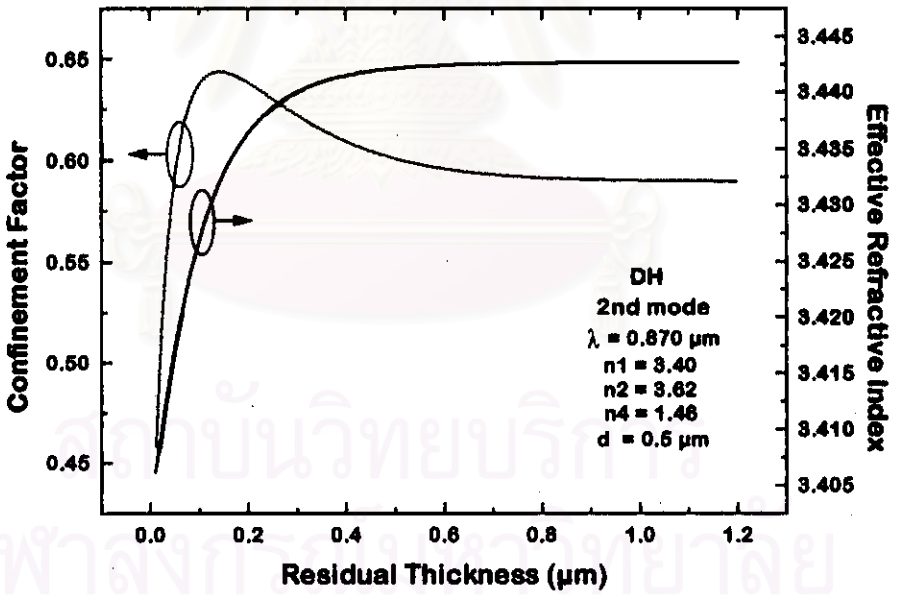

(e-2)

Fig. 4.10 (cont.) Comparison of transverse confinement factor (Γ_T) and effective refractive index (n_e) in various transverse structures (a) DH with 0.1 μm active layer thickness, (b) type-A LOC, (c) type-B LOC, (d) SCH and (e) DH with 0.5 μm active layer thickness. The latter case exists two optical modes (e-1) fundamental and (e-2) second modes. The solid and dotted line are represented to effective refractive index and confinement factor, respectively.

4.4 Lateral analysis of ridge waveguide structure

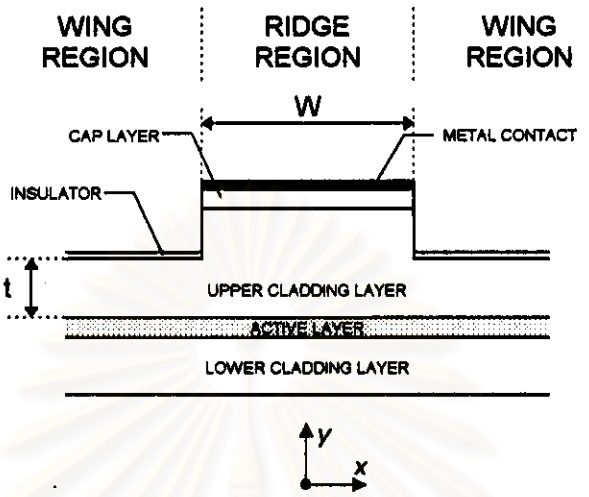

Fig. 4.11 Illustrated schematic of ridge cross section used in the calculation.

Fig. 4.11 is a schematic of the ridge cross section used in the calculation hereafter. In this figure, there are two main design parameters, i.e., the ridge width (w) and the residual thickness of upper cladding layer (t) outside the ridge (wing region). The former mainly prescribes the length in which current injection and optical confinement occurs, while the latter dominates the lateral effective index step, Δn_e.

The effective refractive index of the fundamental transverse mode under the ridge can be computed from the transverse wave equation of Eq.(3.11) by assume that the upper cladding layer is thick enough for the saturated effective refractive index and confinement factor. While the effective index in the wing region, strongly depending on the residual thickness, is calculated and obtained from section 4.1 to 4.3 relying on the transverse structure.

The RW structure can be categorized as index-guided symmetrical three-layer slab waveguide if the residual thickness of both wings is equivalent. The analysis starts from the lateral-mode wave equation [Eq.(3.33)]

$$\frac{\partial^2 E_x}{\partial x^2} + k_o^2 [\, n_e^2(x) - n_L^2 \,] E_x = 0 \qquad (4.30)$$

where

$$n_e(x) = \begin{cases} n_e^{ridge} & , \text{if } |x| \le w/2 \\ n_e^{ridge} - \Delta n_L & , \text{otherwise} \end{cases} \quad (4.31)$$

is the effective refractive index depending on lateral axis (x) and the lateral index step

$$\Delta n_L = n_e^{ridge} - n_e^{wing} \quad (4.32)$$

where n_e^{ridge} and n_e^{wing} are the effective indices corresponding to the ridge and wing region, respectively.

A general solution of Eq.(4.23) according to a symmetrical three-layer problem is

$$E_x = \begin{cases} A\, e^{-\gamma x} & , |x| \ge w/2 \\ B\, cos(\kappa x) & , |x| \le w/2 \end{cases} \quad (4.33)$$

where

$$\gamma = k_o [\, n_L^2 - (n_e^{wing})^2 \,]^{1/2} \quad (4.34)$$

$$\kappa = k_o [\, (n_e^{ridge})^2 - n_L^2 \,]^{1/2} \quad (4.35)$$

The boundary conditions are used to evaluate the eigenvalue equation

$$\frac{\gamma}{\kappa} = \tan(\kappa w/2) \quad (4.36)$$

which the numerical procedure can carry out the lateral effective index (n_L). The portion of laser energy gathered in the ridge is investigated by the lateral confinement factor

$$\Gamma_L = \frac{\int_{-w/2}^{w/2} E_x^2(x)\, dx}{\int_{-\infty}^{\infty} E_x^2(x)\, dx} \quad . \quad (4.37)$$

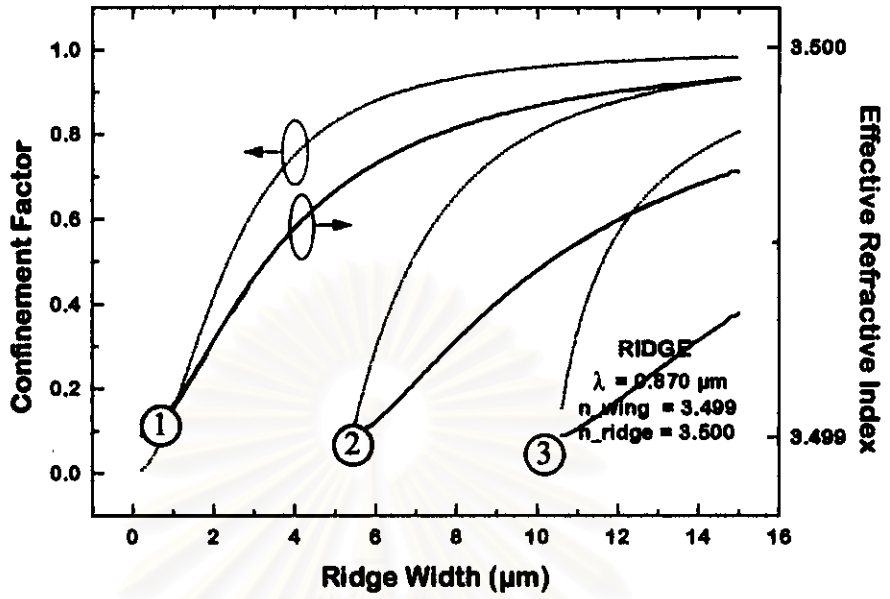

(a)

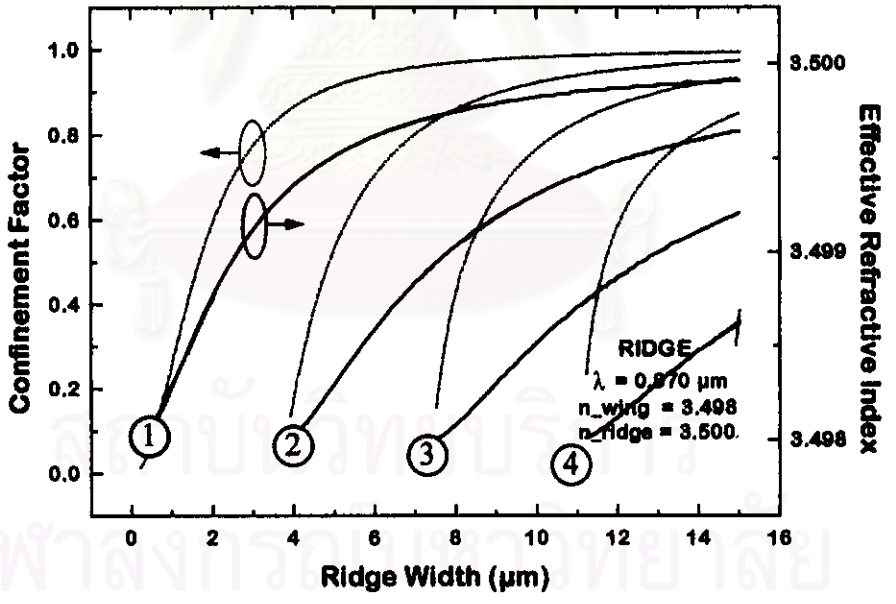

(b)

Fig. 4.12 Simulation results of transverse confinement factor (Γ_T) and effective refractive index (n_e) as the functions of the ridge width (W) for 0.870 μm GaAs ridge lasers with varied lateral index step ($\Delta n_L = n_e^{ridge} - n_e^{wing}$) (a) 0.001, (b) 0.002, (c) 0.005 and (d) 0.010 . The number in the ring is designated to the order of the mode. The solid and dotted line are represented to effective refractive index and confinement factor, respectively.

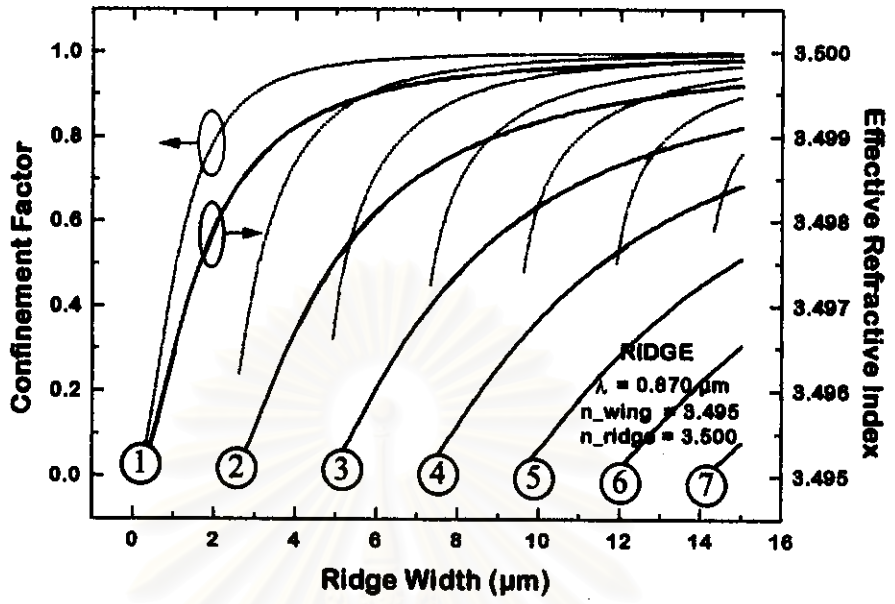

(c)

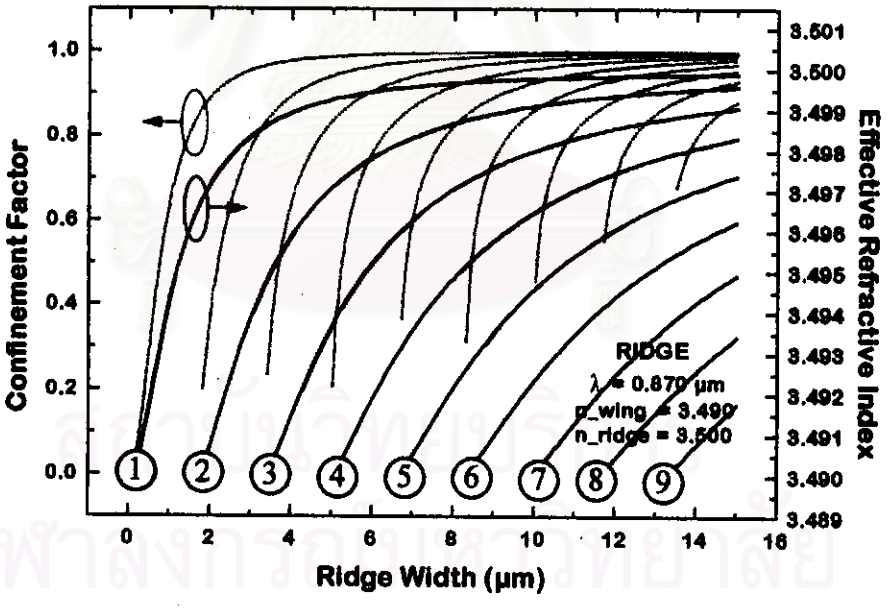

(d)

Fig. 4.12 (cont.) Simulation results of transverse confinement factor (Γ_T) and effective refractive index (n_e) as the functions of the ridge width (W) for 0.870 μm GaAs ridge lasers with varied lateral index step ($\Delta n_L = n_e^{ridge} - n_e^{wing}$) (a) 0.001, (b) 0.002, (c) 0.005 and (d) 0.010. The number in the ring is designated to the order of the mode. The solid and dotted line are represented to effective refractive index and confinement factor, respectively.

The simulation results of the lateral effective index and confinement factor are calculated in the function of the lateral index step (Δn_L) and the ridge width (w). For a RW laser with the constant ridge effective index (n_e^{ridge}) of 3.500 and varied lateral index step, the lateral effective indices (n_L) and confinement factor (Γ_L) can be achieved numerically as shown in Fig. 4.12. In each figure, the lateral index step of 0.001 (Fig.4.12a), 0.002 (Fig.4.12b), 0.005 (Fig4.12c) and 0.010 (Fig.4.12d) have 3, 4, 7 and 9 modes appeared within 15 μm of ridge width (W). It means that the increase of index step produces the undesired higher modes and also reduces the mode discrimination of the ridge waveguide. It should be realized that the less lateral index step is to enhance the ridge width maintaining single mode operation which also produces the higher confined power in lateral direction. Anyway, the least index step is obtained by the exact residual thickness which requires a precise etching control to establish the ridge.

The other consideration of the lateral index step is the significant variation of refractive index with the injected current which occurs in the ridge region [8,54]. The current-induced index will typically reduce the refractive index of the active layer by 10^{-2}, which in turn reduces the cold-cavity effective index by about 10^{-3}. For this reason, a cold-cavity lateral index step greater than 3×10^{-3} is desired to provide lateral mode stability [8] which maintains the index guiding in a ridge waveguide laser.

Fig. 4.13 shows two designed parameters (i) residual thickness in wing region (t) which affect lateral index step (Δn_L) and (ii) cut-off ridge width (W_{co}) which is the maximum ridge width maintaining fundamental lateral-mode operation. From the figures, it is obvious that reduction of index step by increasing of residual thickness will enhance mode discrimination (wider cut-off ridge width). There are 5 transverse structures used for comparisons (a) DH with 0.1 μm active layer thickness, (b) DH with 0.5 μm active layer thickness, (c) type-A LOC, (d) type-B LOC, and (e) SCH. At the same residual thickness, the cut-off width will be sorted descending as DH (0.5 μm), SCH, LOC-A, LOC-B and DH (0.1μm). It should be reminded that DH with 0.5 μm active layer thickness has two transverse modes as shown in section 4.1. Then the most preferable transverse structure to support the single mode operation is SCH because it can provide higher confined power from its wider ridge width which is not exceed the cut-off ridge width (W_{co}).

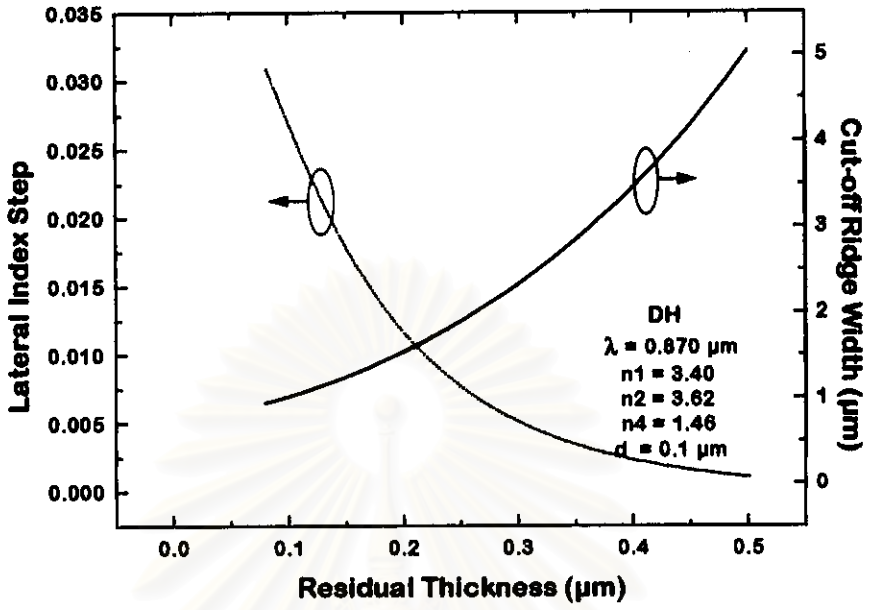

(a)

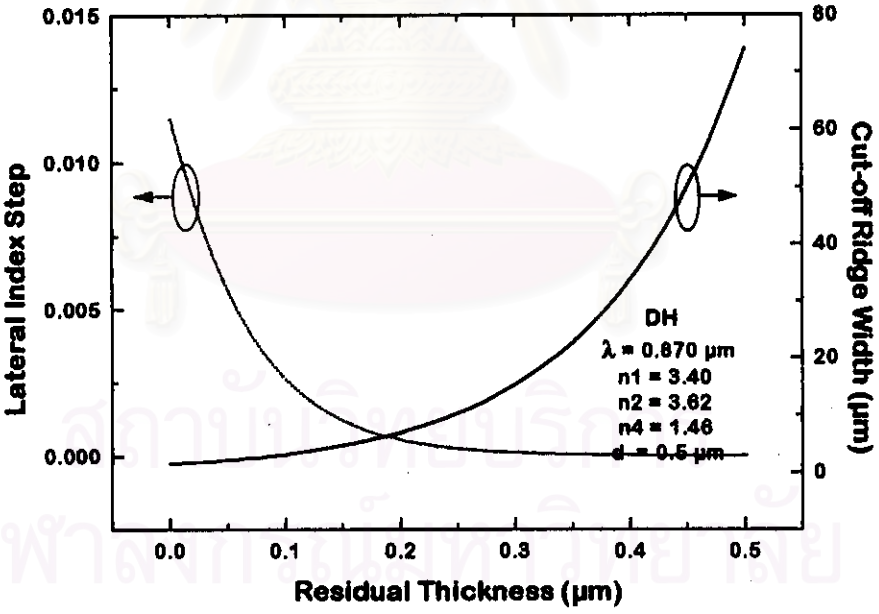

(b)

Fig. 4.13 Simulation results of lateral index step (Δn_L) and cut-off ridge width (W_{co}) as the functions of the residual upper cladding layer thickness (t) for 0.870 μm GaAs laser in various transverse structures (a) DH with 0.1 μm active layer thickness, (b) DH with 0.5 μm active layer thickness, (c) type-A LOC, (d) type-B LOC and (e) SCH . The solid and dotted line are represented to effective refractive index and confinement factor, respectively.

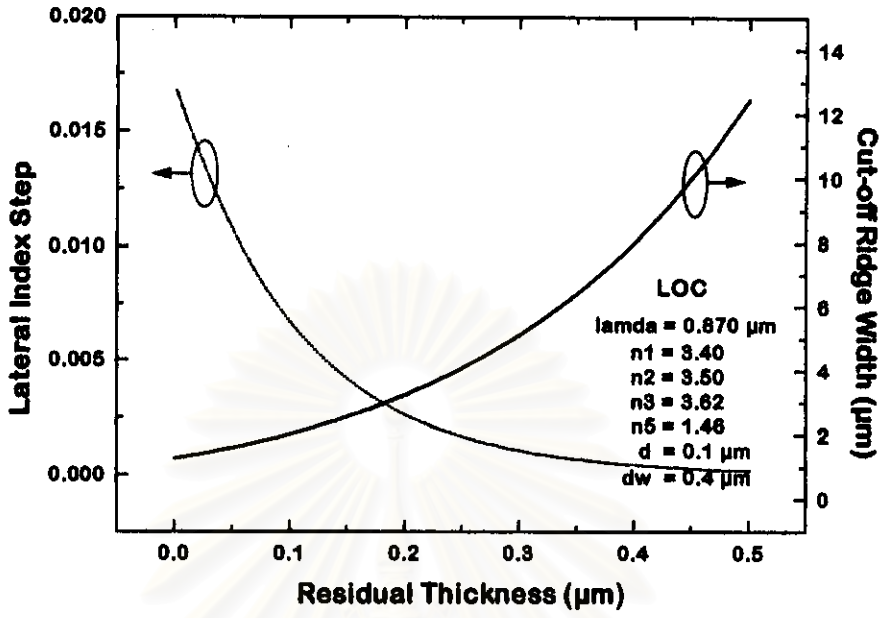

(c)

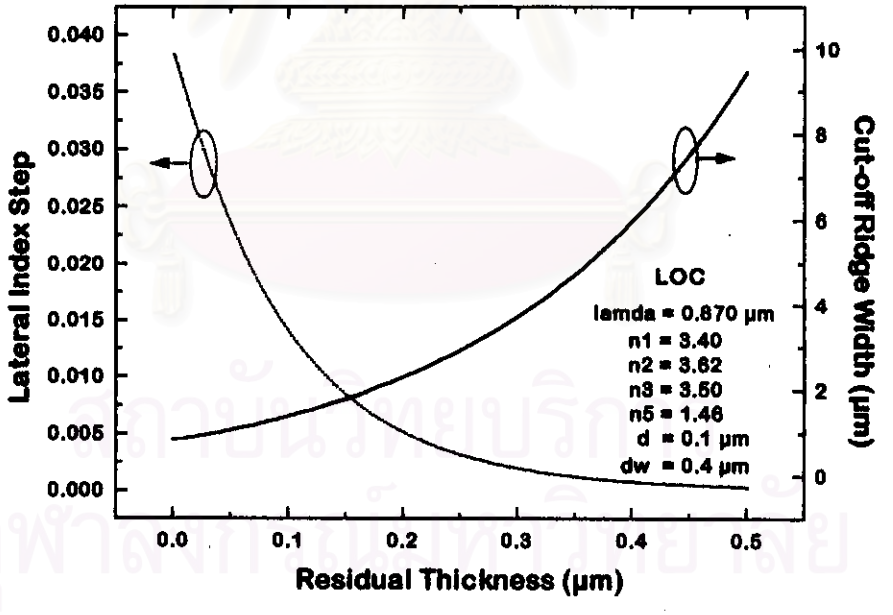

(d)

Fig. 4.13 (cont.) Simulation results of lateral index step (Δn_L) and cut-off ridge width (W_{co}) as the functions of the residual upper cladding layer thickness (t) for 0.870 μm GaAs laser in various transverse structures (a) DH with 0.1 μm active layer thickness, (b) DH with 0.5 μm active layer thickness, (c) type-A LOC, (d) type-B LOC and (e) SCH . The solid and dotted line are represented to effective refractive index and confinement factor, respectively.

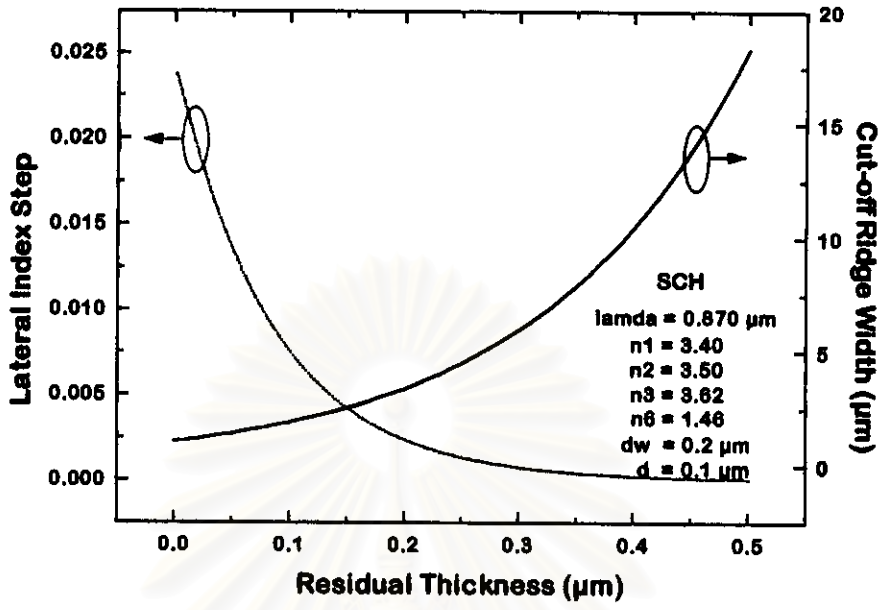

(e)

Fig. 4.13 (cont.) Simulation results of lateral index step (Δn_L) and cut-off ridge width (W_{co}) as the functions of the residual upper cladding layer thickness (t) for 0.870 μm GaAs laser in various transverse structures (a) DH with 0.1 μm active layer thickness, (b) DH with 0.5 μm active layer thickness, (c) type-A LOC, (d) type-B LOC and (e) SCH. The solid and dotted line are represented to effective refractive index and confinement factor, respectively.

4.5 Proposed ridge waveguide structure

Due to a limitation of LPE process used in SDRL, the transverse structure was fabricated to be Double Heterostructure (DH) with active layer thickness of 0.1 μm. The refractive indices of both upper and lower cladding layers are set to 3.40 and the index of active layer is set to 3.62. Ridge region consists of upper cladding layer greater than 1.2 μm thickness to produce its stable effective refractive index (n_e^{ridge}) of 3.436 (see Fig. 4.2b), and wing regions consist of residual thickness of 0.35 μm to produce its refractive index (n_e^{wing}) of 3.433, then the cold-cavity lateral index step is obtained at 0.003 which provides the operating index step (Δn_L) of 0.002. The last parameter is the ridge width which is not exceed cut-off ridge width (W_{co}) of 4 μm (see Fig. 4.13a). All parameters of this proposed structure are shown in Fig. 4.14.

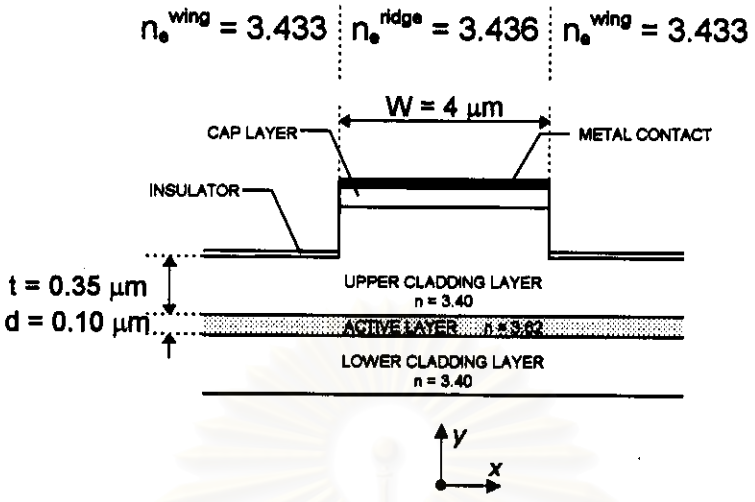

Fig. 4.14 Cross-section schematic of the proposed ridge waveguide laser.